Star formation

Protostellar Collapse and Pre-Main-Sequence Evolution

Full simulation of gravitational collapse

- Parameters of the presolar nebula:
  - Mass > $1M_\odot$
  - T = 10 K (like other sources)
  - R = 0.05 pc (=10,000 AU; critical radius of Bonnor-Ebert sphere)
  - $\langle n(H_2)\rangle = 10^4$ cm^{-3}
  - $t_{ff} = 1.9\ 10^5$ yrs
- Proto-Sun:
  - Solar radius 0.005 AU – factor 2 10^7
  - Solar density – factor 10^{20}
  - Solar temperature – factor 10^6

→ Problem with dynamic range of numerical codes
→ Full direct simulation still impossible

Computation of full dynamics

- Collapse of initially static cloud of uniform density
- No magnetic field
- No rotation

  $\rightarrow$ 1-dimensional problem

- Trajectories of particles: $$\ddot{r} = -\frac{Gm}{r^2}$$
- Parametric solution: $$r = r_0 \cos\zeta$$ $$t = \left(\frac{8\pi G\rho_0}{3}\right)^{-1/2} (\zeta + 1/2 \sin 2\zeta)$$
- $\rightarrow$ Contraction to point mass at $$\zeta = \pi/2$$ $$t = \tau_{ff} = \left(\frac{3\pi}{32G\rho_0}\right)^{1/2}$$

Dynamics of a spherical cloud

$$\frac{\partial u}{\partial t}+u\frac{\partial u}{\partial r}+\frac{1}{\rho}\frac{\partial P}{\partial r}+\frac{GM_r}{r^2}=0$$

(force equation, Eulerian form)

$$\frac{\partial \rho}{\partial t}+\frac{1}{r^2}\frac{\partial}{\partial r}\left(r^2\rho u\right)=0$$

(mass continuity)

$$\frac{\partial M}{\partial t}+u\frac{\partial M}{\partial r}=0, \quad \frac{\partial M_r}{\partial r}=4\pi r^2\rho$$

Many possible solutions possible following from different initial density structures. e.g.

- Larson-Penston relation (last lecture)
- Singular isothermal sphere
- ...

Protostellar collapse: structure

Evolution of global density structure:

- Homologous collapse:

$$\rho(r,t) = \rho_0(r) \times \frac{A(t)}{A(t_0)}$$

  - Ideal case
  - Never practically met

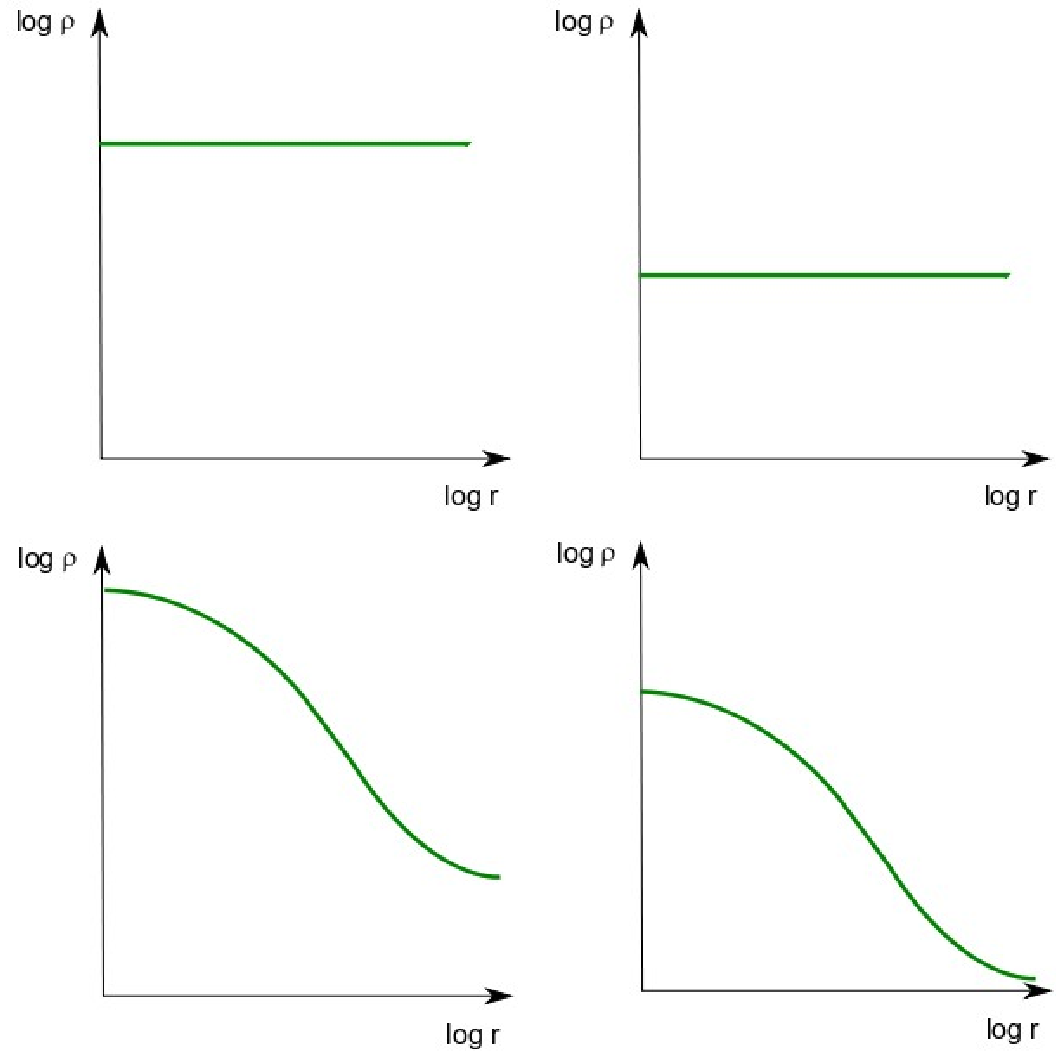

Protostellar collapse: structure

Evolution of global density structure:

- Non-homologous collapse:

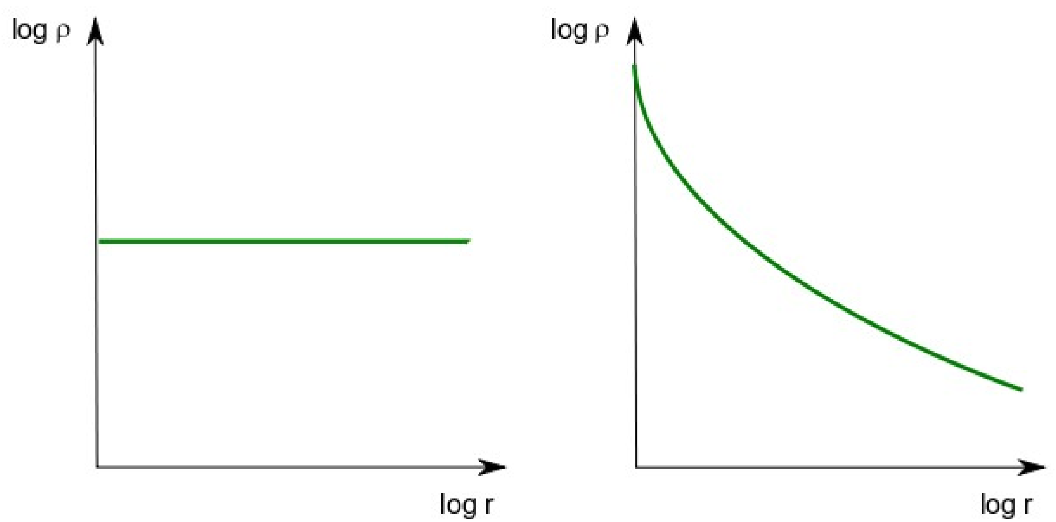

ρ

- General solution for arbitrary initial conditions

Protostellar collapse: structure

Evolution of global density structure:

- Self-similar collapse:

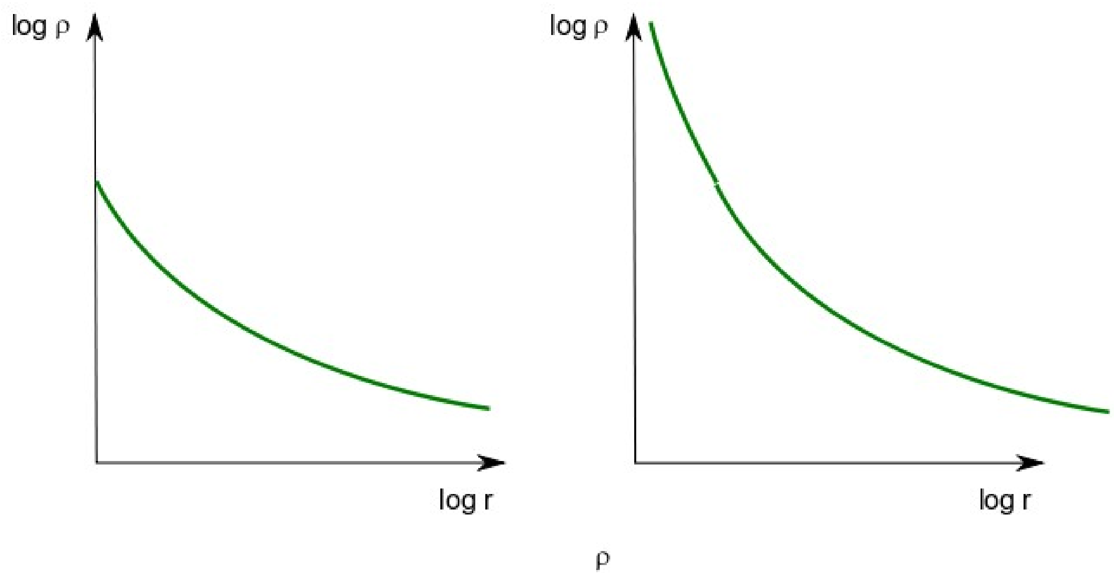

$$\rho(r,t) = \rho(r/t)$$

  - Simple "shift" in r

  - Solution for SIS initial condition
  - General solution as soon as singularity has formed
  - Density structure can expressed as function of $x = \dfrac{r}{c_s t}$

Similarity solution

$$x = \frac{r}{c_s t} \quad \text{(dimensionless)}$$

$$u(r,t) = c_s v(x) \qquad \rho(r,t) = \frac{\alpha(x)}{4\pi G t^2} \qquad M(r,t) = \frac{c_s^3 t}{G} m(x)$$

momentum and density continuity can be written

$$\left[(x-v)^2 - 1\right] v' = \left[\alpha(x-v) - \frac{2}{x}\right](x-v)$$

$$\left[(x-v)^2 - 1\right] \frac{\alpha'}{\alpha} = \left[\alpha - \frac{2}{x}(x-v)\right](x-v)$$

Advantage: only one variable, x, not two, r and t

Inserting into the Mass equations yields

$$m = m'(x-v), \quad m' = x^2 \alpha$$

$$\Rightarrow \quad m = \alpha x^2 (x-v)$$

Initial cloud structure

Trivial solution $v=0$:

$$\alpha=\frac{2}{x^2}$$

corresponds to static singular isothermal sphere

General solution: initially cloud at rest

$$t\rightarrow 0 \Rightarrow x\rightarrow\infty \text{ and } v=0$$

then the equations become

$$v'=\alpha-\frac{2}{x^2} \qquad \alpha'=\frac{\alpha(\alpha-2)}{x}$$

Asymptotic solutions

For $x \to \infty$ (large radii or shortly after start of infall)

$$\alpha \to \frac{A}{x^2} \quad v \to -\frac{A-2}{x} \quad m \to A\,x$$

the constant A has to be $>2\,($infall, $v<0)$
to start the collapse, but not much larger

$$\rho(r,t) = \frac{c_s^2 A}{4\pi G r^2}$$

$$u(r,t) = 0$$

$$M(r,t) = \frac{A c_s^2}{G} r$$

can be used as boundary for numerical integration.

Asymptotic solutions

$x \to 0 \, (t \to \infty)$: $\quad |v| \gg 1 \quad \alpha x |v| \gg 1$

one then finds

$$v' = \alpha \text{ and } v'' + \frac{v'^2}{v} + \frac{2v'}{x} = 0$$

which is solved for $x \to 0$ by

$$\alpha \to \sqrt{\frac{m_0}{2x^3}} \quad v \to -\sqrt{\frac{2m_0}{x}} \quad \text{where } m_0 = -(x^2 \alpha v)_{x=0}$$

cont'd

$$\rho(r,t)=\sqrt{\frac{m_0 c_s^3}{32\pi^2 G^2}}\,t^{-1/2} r^{-3/2}$$

$$u(r,t)=-\sqrt{2\mathrm{m}_0 c_s^3}\,t^{1/2} r^{-1/2}$$

With the central mass

$$M_*(t)=\frac{m_0 c_s^3}{G}t$$

$$u(r,t)=-\sqrt{\frac{2GM_*(t)}{r}}$$ (free-fall velocity)

and the accretion rate

$$\dot{M}=4\pi r^2 \rho u=\frac{m_0 c_s^3}{G}$$

Inside-out collapse

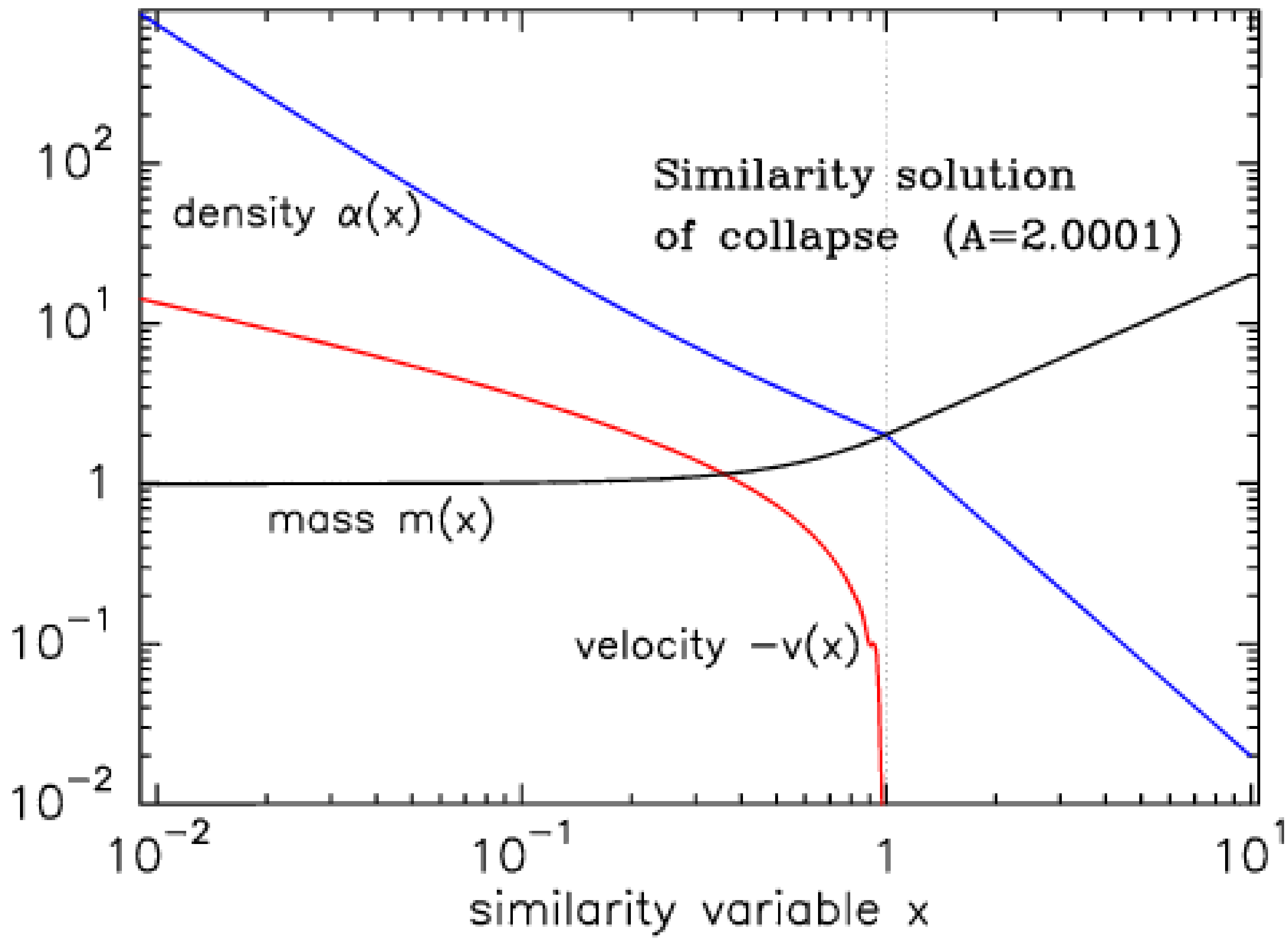

Shu-type collapse

TABLE III. Properties of the Shu solution of isothermal collapse.

	Before core formation ($t<0$)	After core formation ($t>0$)
Density profile	$\rho \propto r^{-2}$, $\forall r$ singular isothermal sphere	$\rho \propto r^{-3/2}$, $r \leqslant c_s t$ $\rho \propto r^{-2}$, $r > c_s t$
Velocity profile	$v \equiv 0$, $\forall r$	$v \propto r^{-1/2}$, $r \leqslant c_s t$ $v \equiv 0$, $r > c_s t$
Accretion rate		$\dot{M} = 0.975 c_s^3 / G$

Properties of the solution

- A=2 → SIS, stable
- Collapse as soon as A=2 is exceeded
- At large radii, the original r^{-2} density profile is preserved
- At small radii, the density profile is flatter
- In the envelope, the gas is at rest and does not know that the center is collapsing
- In the core, the velocities are supersonic and approach the free-fall velocity
- The accretion rate is time-independent
- At the transition region between free-falling core and static envelope, $x=1$ and $r=c_s t$, so it is moving outward with the speed of sound

Shu-type collapse

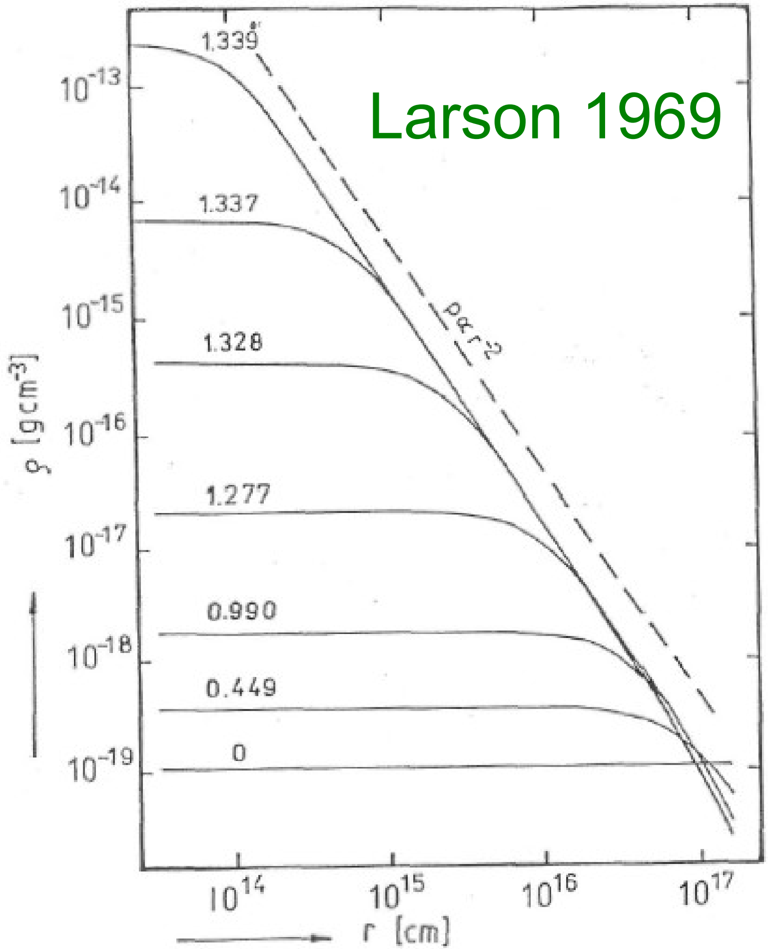

Abbildung 6.2: Zeitliche Veränderung der Dichteverteilung im klassischen Kollapsmodell von Larson (1969). Die Zeit ist in Einheiten von 10^{13} s angegeben.

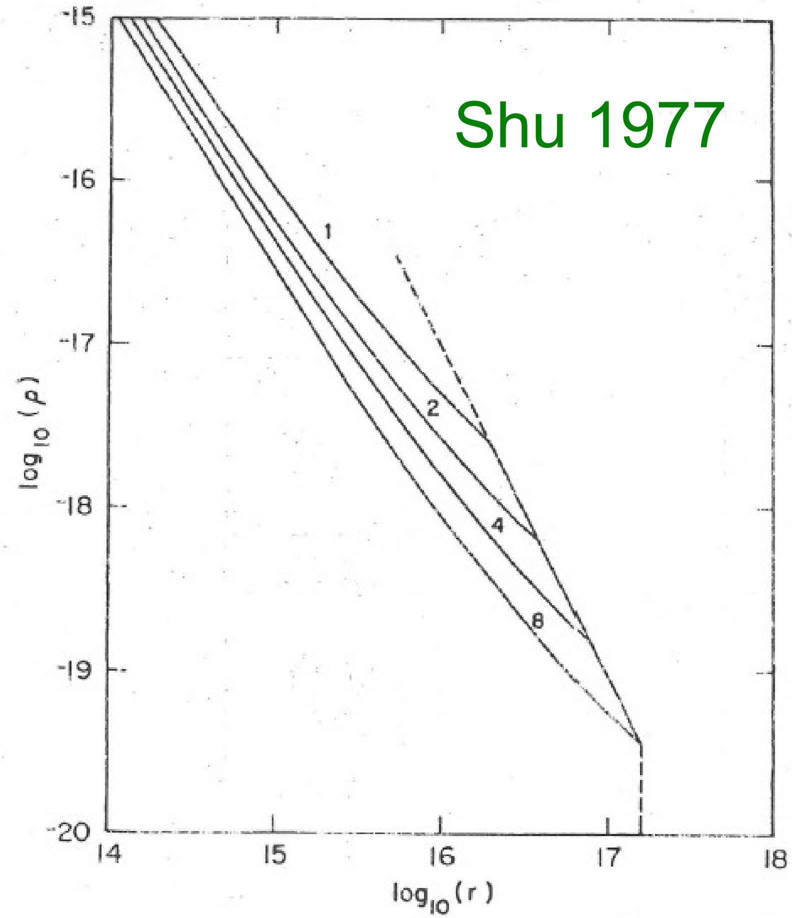

FIG. 3.—Expansion-wave collapse solution for a 0.96 $M_\odot$ singular sphere with $a = 0.2$ km s^{-1} and $P_{ext}/k = 1.1 \times 10^5$ cm^{-3} K. The initial radius of the outer boundary is indicated by the vertical dashed lines. (*a*) The density profiles at $t =$ 1, 2, 4, and 8 $\times 10^{12}$ s. (*b*) The velocity profiles at t = 1, 2, 4, and 8 $\times 10^{12}$ s. The dimensions of r, ρ_0 and u are cm, g cm^{-3}, and cm s^{-1}, respectively.

Missing items

- Rotation
- Non-isothermality
- Magnetic fields

Energies

Parental cloud:

gravitational Energy $E_{grav} = \frac{GM^2}{R} \approx 2\,10^{42}\,\mathrm{erg}$

thermal Energy $E_{therm} = \frac{3\,k\,T\,M}{2\mathrm{m}} = 1\,10^{42}\,\mathrm{erg}$

sun as a protostar $R = 2\,R_{\odot}$ (T Tauri stars)

gravitational Energy $E_{grav} = \frac{GM^2}{2\,R_{\odot}} \approx 2\,10^{48}\,\mathrm{erg}$

half of which went into heating: $T \approx 3\,10^6\,\mathrm{K}$
the other half was radiated away,
this gives for $t = t_{ff}$: $\langle L \rangle \approx 40\,L_{\odot}$

Rotational energy

Galaxy rotates differentially, with $\frac{dv}{dR_0} \approx -5\, km\, s^{-1}\, kpc^{-1}$

which leads to angular momentum for clouds

$$E_{rot} = \frac{1}{2} I\, \omega^2 \approx 10^{37}\,\mathrm{erg}$$

$I = \frac{2}{5} M\, R^2$ for a sphere of constant density

but the angular momentum $I\,\omega$ is conserved

therefore $E_{rot} = \frac{1}{2} \frac{(I\,\omega)^2}{I} \propto \frac{1}{R^2}$

which would increase the rotational Energy by 10^{14}

Magnetic energy

- The cloud can only collapse if the magnetic Energy is smaller than the gravitational, i.e.

$$\frac{3GM^2}{5\,R} > \frac{R^3\,B^2}{3}$$

Which implies the existence of a minimum Mass for instability in the presence of a magnetic field

$$M_{mag} = \frac{5^{3/2}}{48\,\pi^2\,G^{3/2}}\,\frac{B^3}{\rho^2}$$

Energies

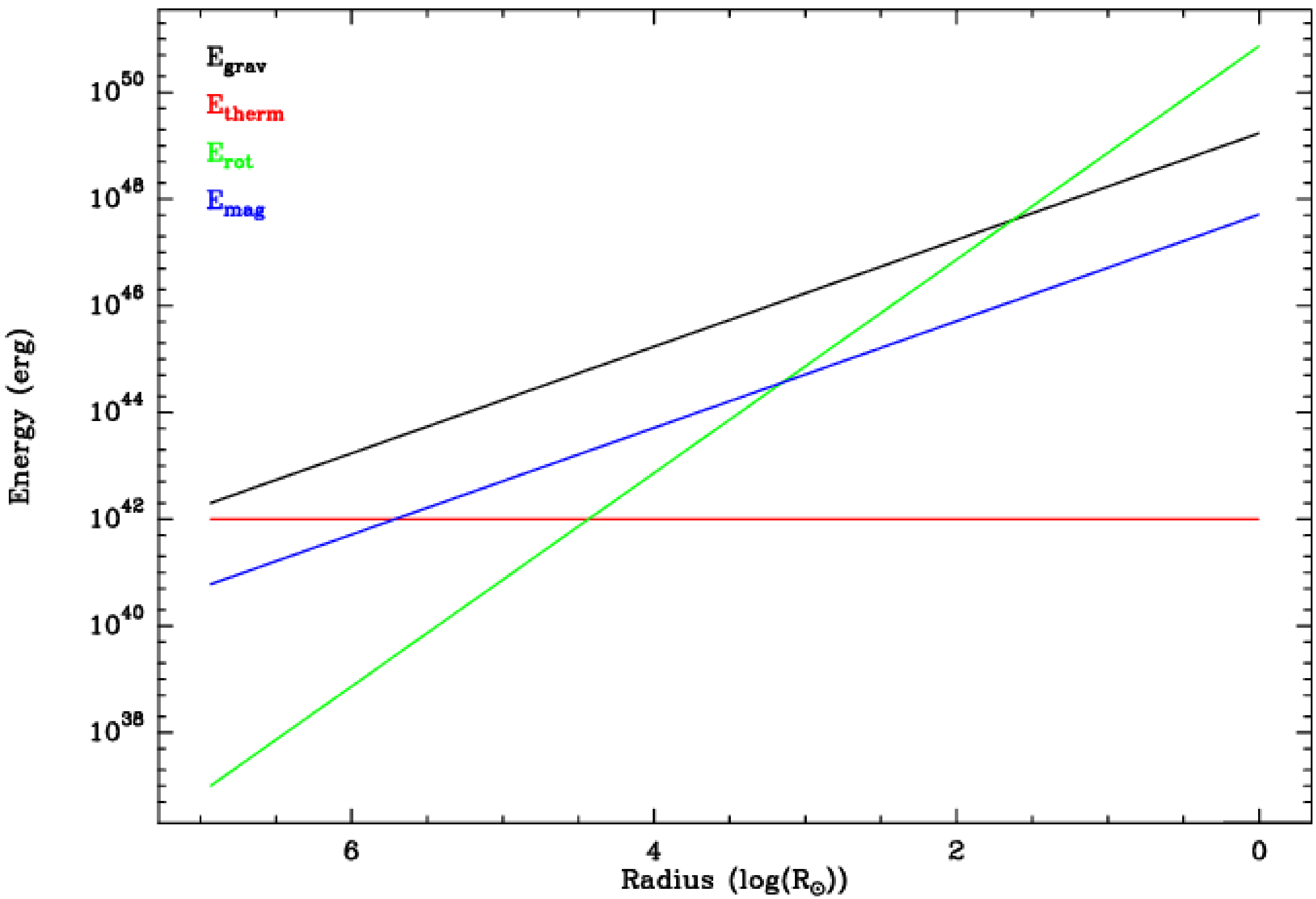

E_{grav}
E_{therm}
E_{rot}
E_{mag}
10^{50}
10^{48}
10^{46}
10^{44}
10^{42}
10^{40}
10^{38}
Energy (erg)
6
4
2
0
Radius (log($R_\odot$))

Magnetic energy

$$E_{mag} = \frac{B^2}{8\pi} \frac{4\pi}{3} R^3 \approx 6\,10^{40}\,\text{erg for}\;\; B = 10\,\mu G$$

because of magnetic flux conservation $BR^2 = \text{const}$ and

$$E_{mag} \propto \frac{(BR^2)^2}{R}$$

which would make $B \approx 10^{13}$ times stronger in the star which is not observed

Is the Field frozen?

- Generally not, since the ionization fraction is low (10^{-4}-10^{-7}) in interstellar clouds

→ ambipolar diffusion

Ambipolar diffusion

- Consider ions static (frozen) and the neutrals subject to the gravitational field, then the force balance is

$$\frac{GM}{R^2} n_n m = n_i n_n \langle \sigma u \rangle m w_d$$ where

n_n, n_i are the densities of neutrals and ions

$\langle \sigma u \rangle$ is the effective cross section

w_d is the drift speed between the two components

Resulting ambipolar diffusion time:

$$t_{ad} = \frac{R}{w_d} = \frac{n_i}{n_n} \frac{3}{4\pi G m} \langle \sigma u \rangle \approx 2\,10^{13} \frac{n_i}{n_n} [\mathrm{yr}]$$

Ambipolar diffusion

- With an ionization rate of 10^{-7}, that corresponds to several million years
- Collapse along the field lines is not inhibited
  - this leads to flattened structures perpendicular to the magnetic field
  - But support due to excited Alfvèn waves
- There is some drag of the neutrals to the ions, so the field lines will be pinched
- Magnetic braking is also capable of removing an-gular momentum

Observations of magnetic fields

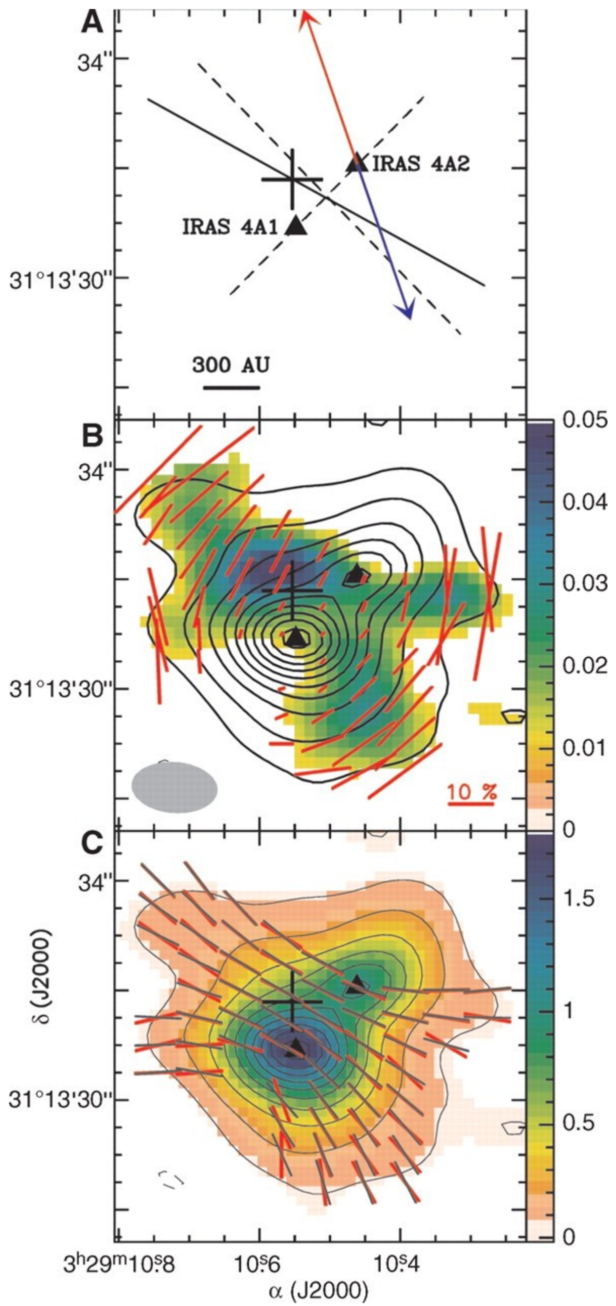

Fig. 1. (A) Sketch of the axis directions: red/blue arrows show the direction of the redshifted/blueshifted lobes of the molecular outflow, probably driven by IRAS 4B (8); solid lines show the main axis of the magnetic field; and dashed lines show the envelope axes. The solid triangles show the positions of IRAS 4A1 and 4A2. The cross shows the center of the magnetic field symmetry. (B) Contour map of the 877-μm dust emission (Stokes I) superposed with the color image of the polarized flux intensity. Red vectors indicate that length is proportional to fractional polarization, and the direction is the position angle of linear polarization. Contour levels are 1,3,6,9,...30 x 65 mJy per beam. The synthesized beam is shown in the bottom left corner. (C) Contour and image map of the dust emission. Red bars show the measured magnetic field vectors. Gray bars correspond to the best-fit parabolic magnetic field model. The fit parameters are the position angle of the magnetic field axis {theta}PA = 61° ± 6°;the center of symmetry of the magnetic field {alpha}0(J2000) = 3h 29 m 10.55 s ± 0.06 s and {delta}0(J2000) = 31°13'31.8" ± 0.4"; and C = 0.12 ± 0.06 for the parabolic form y = g + gCx2, where the x is the distance along the magnetic field axis of symmetry from the center of symmetry.

Shu-type collapse

- Ambipolar diffusion allows the creation of a Singular Isothermal Sphere, which becomes supercritical
- Then collapse stars from this quasi-static configuration
- Inside-out collapse
- Accretion rate governed by effective velocity

$$c_s \longrightarrow v_{eff} = \sqrt{c_s^2 + v_A^2 + v_T^2}$$

$$\rightarrow \qquad \dot{M} = m_0 \frac{v_{eff}^3}{G}$$

- Typical values: 10^{-6}-10^{-5} $M_\odot$/a
- Duration of accretion phase: 10^5-10^6 a

Collapse in 2-D or 3-D

- Allows to fully include magnetic field and rotation
  - Always creating disk structures
- Still very limited dynamic range

- Centrifugal force creates an accretion disk

- Magnetic fields and rotation create hierarchy of disks

Hydrodynamic 2-D collapse simulation by Tscharnuter (1987)

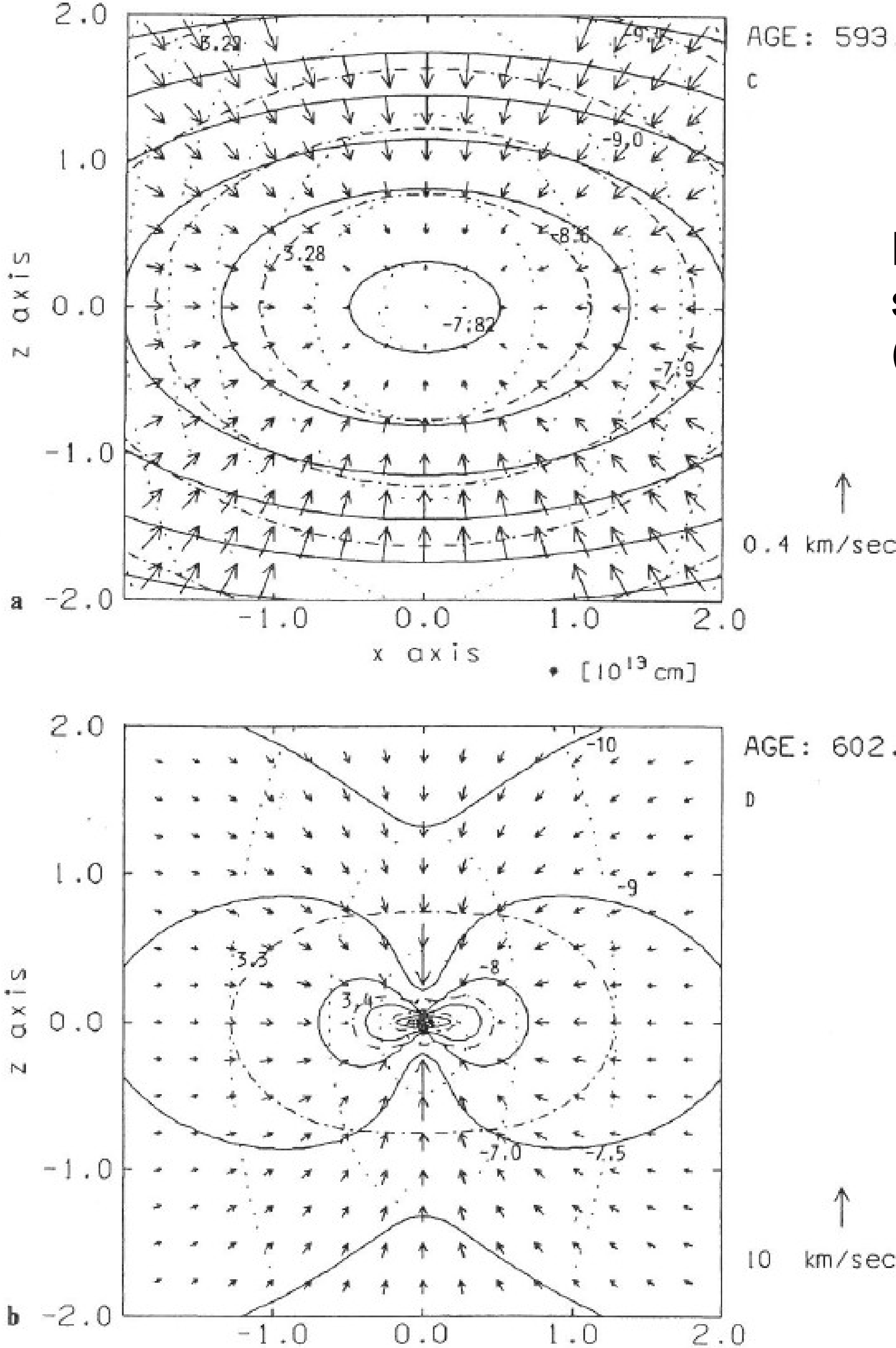

Fig. 7a and b. Meridional cross-sections at the beginning of the second collapse (point *C*) and at the beginning of the bounce (point *D*). Full lines are contours of constant density, dash-dotted lines and dotted lines refer to the temperature and angular velocity, respectively. The numbers given on the plot are logarithms of density (right upper side), temperature (left upper side), and angular velocity (right lower side). Arrows indicate the (projected) velocity field, the single arrow on the right hand side gives the scale

Galli & Shu 1993

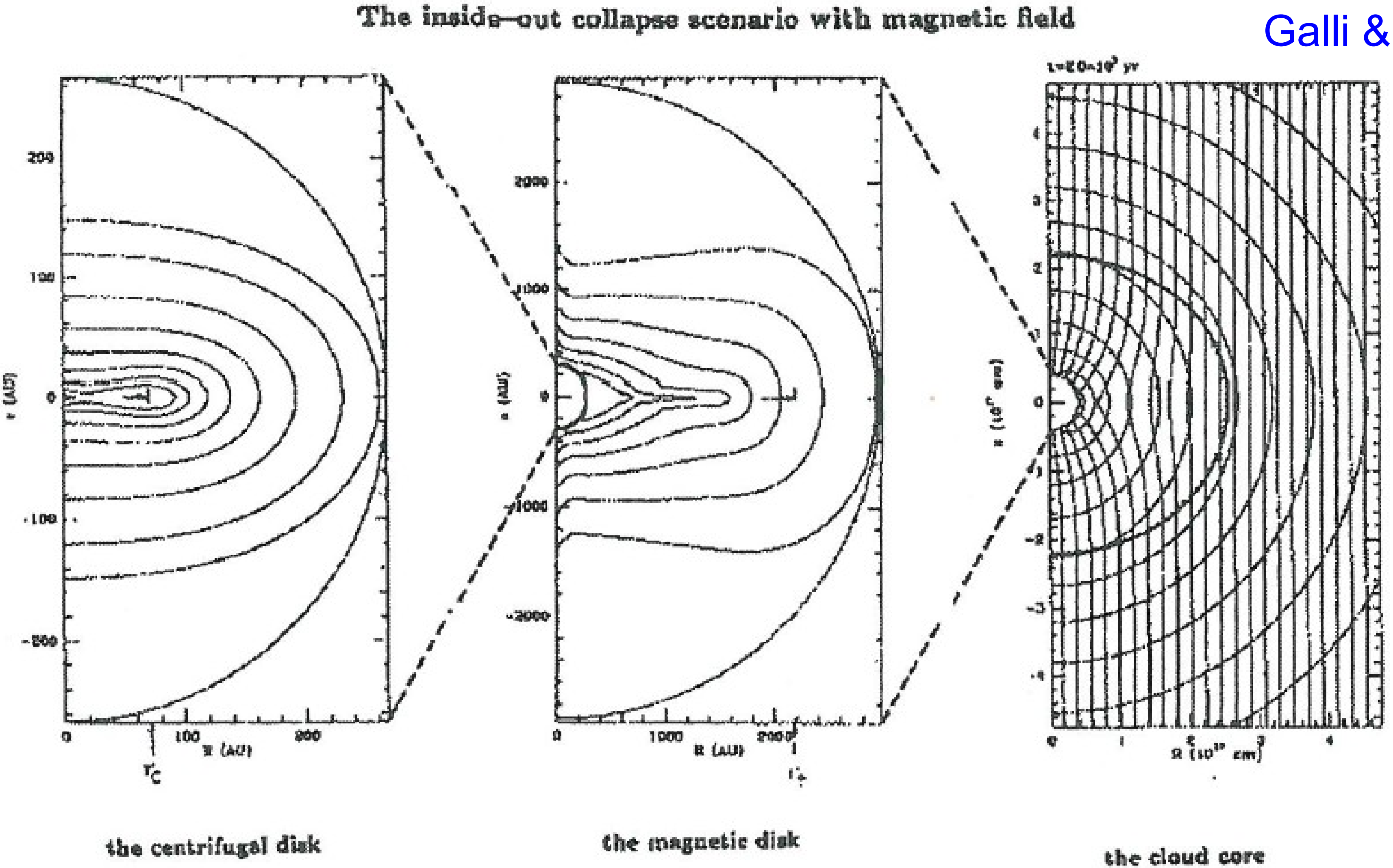

Fig. 2. Global view of the collapse of a magnetized, rotating dense core. The right panel shows the isodensity contours and magnetic field lines over a scale of about 0.1 pc. The dotted line represents the infall magnetosonic wave that propagates faster in the direction perpendicular to the field. In the middle panel, on scales of $\sim 10^3$ AU, the dynamics is dominated by magnetic and gravitational forces that shape the density distribution in the equatorial plane. The left panel shows the isodensity contours in the innermost $\sim 10^2$ AU. The positions of r_B and r_C (see text) are indicated in the middle and left panels. (Adapted from Galli & Shu [17])

Collapse in 2-D or 3-D

- Time scales for central collapse only slightly changed:
  - Replace $c_s \longrightarrow v_{eff} = \sqrt{c_s^2 + v_A^2 + v_T^2}$
- New parameter for detailed evolution:
  - β - specific angular momentum
  - + Normal parameters:
    - α – thermal to gravitational energy
    - M, T – mass and temperature

$$\beta = \frac{L}{M} = \frac{\omega^2}{4\pi G\rho}$$

$$\alpha = \frac{U}{W} = \frac{5}{2}\frac{kTR}{GM}$$

Collapse in 3-D

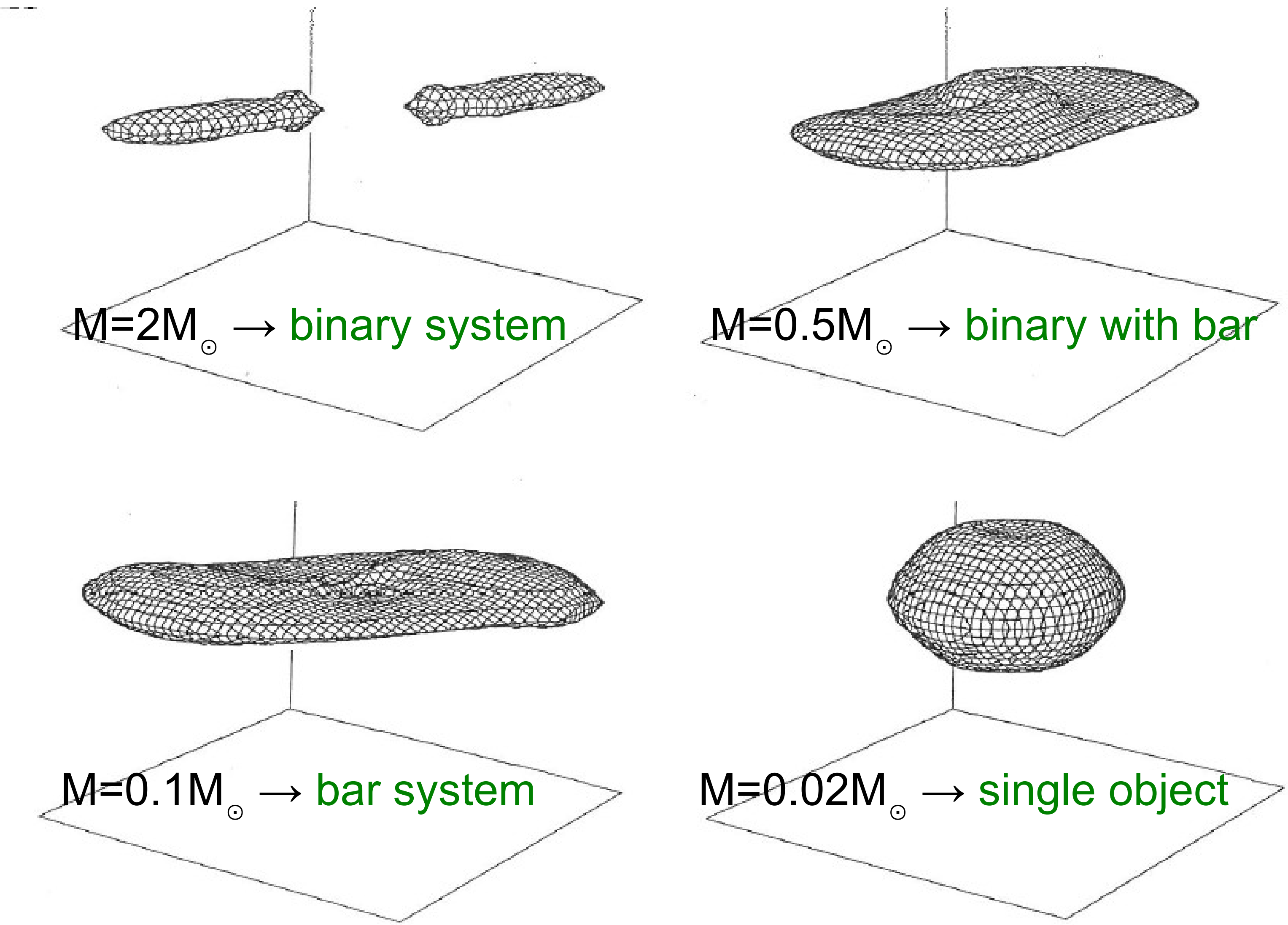

FIG. 2.—Examples of the four different types of solutions encountered in the calculations: (*a*) binary, (*b*) binary-bar, (*c*) single-bar, and (*d*) single. Each plot shows a three-dimensional surface with constant density in the central region (box size = B) of a given model. (*a*) binary: model 8, $\rho = 5 \times 10^{-14}$ g cm^{-3}, $B = 360$ AU; (*b*) binary-bar: model 55, $\rho = 10^{-13}$ g cm^{-3}, $B = 96$ AU; (*c*) single-bar: model 6, $\rho = 10^{-12}$ g cm^{-3}, $B = 38$ AU; (*d*) single: model 3, $\rho = 10^{-11}$ g cm^{-3}, $B = 15$ AU.

Boss (1986)

α=0.25
β=0.04
T=10K

Collapse in 3-D

- Fragmentation
  - Already discussed for stability
  - Occurs also during the collapse within the disk

$$M_J = \frac{\pi}{32}\sqrt{\frac{3}{2}}\left(\frac{\pi k}{4m}\right)^{3/2}\frac{T^{3/2}}{\rho^{1/2}}$$

$$\tau_{ff} = \left(\frac{3\pi}{32G\rho_0}\right)^{1/2}$$

  - In isothermal collapse the Jeans mass decreases at growing density

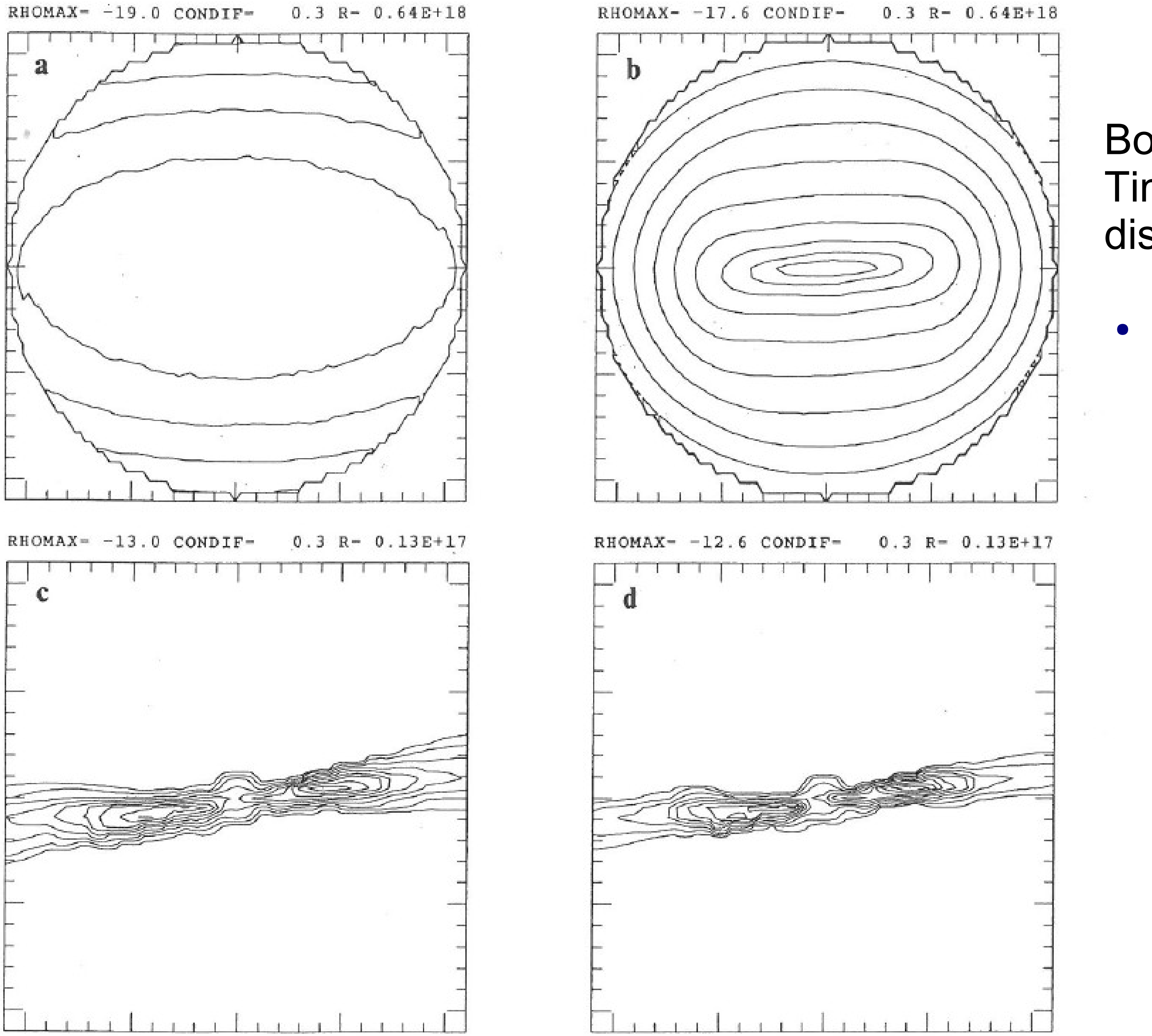

FIG. 2.—Density contours in the equatorial plane for model I4 at four different times: (*a*) $0.0t_{ff}$; (*b*) $1.006t_{ff}$; (*c*) $1.181t_{ff}$; and (*d*) $1.183t_{ff}$. A region of diameter 1.3×10^{18} cm spanning 101 radial grid points is shown in (*a*) and (*b*), while a region of diameter 2.6×10^{16} cm spanning 15 radial grid points is shown in (*c*) and (*d*). Contours correspond to factors of 2 change in density. Maximum densities (log) in g cm^{-3} are noted on each frame. The initially prolate cloud (*a*) forms an intermediate cylinder (*b*), which continues to collapse and become extremely narrow, eventually fragmenting into a binary (*c*) or possibly a higher order system (*d*).

Boss (1993)
Time evolution of disk

- Large angular momentum

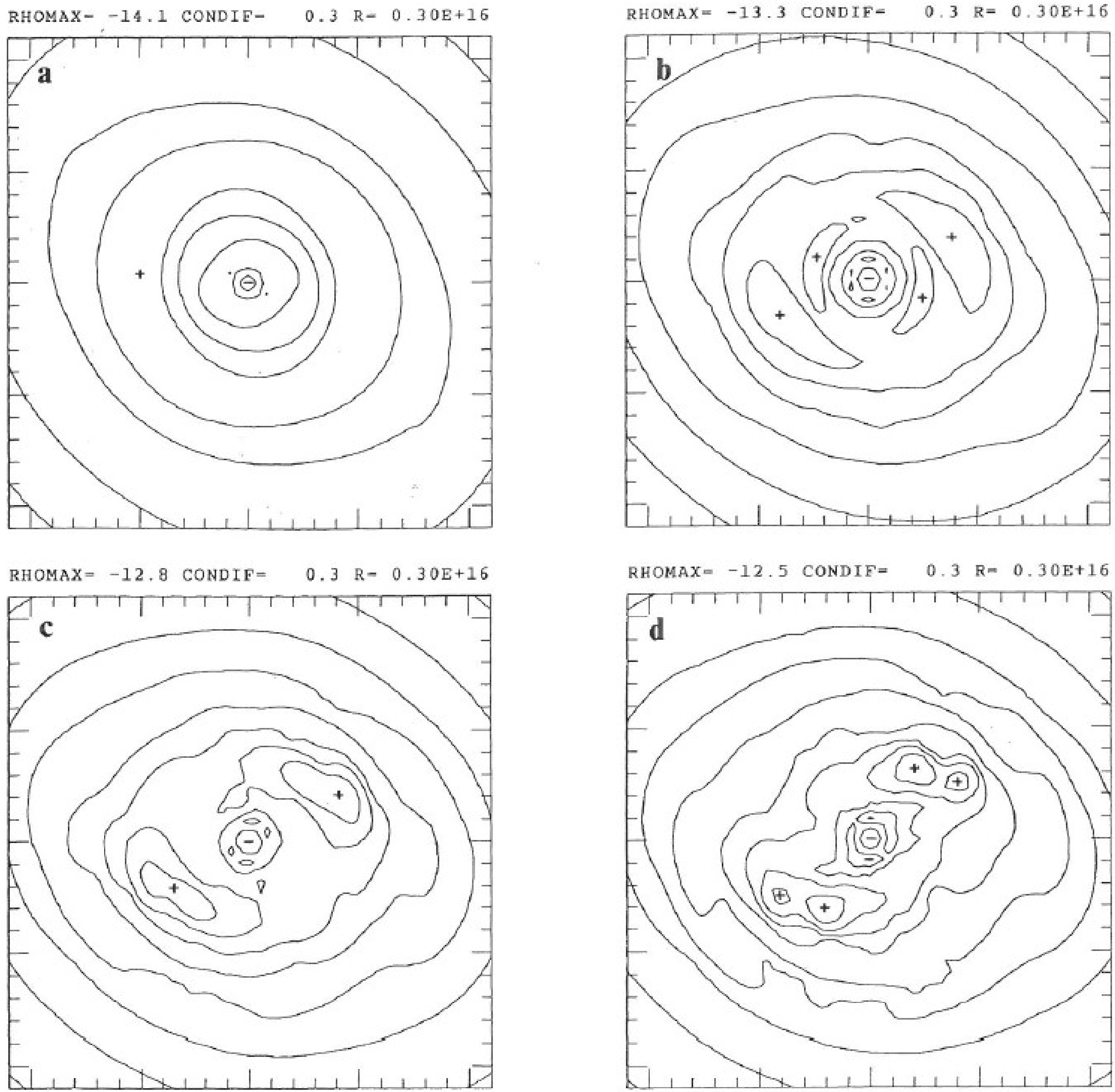

FIG. 1.—Density contours in the equatorial plane for model C4-ST at four different times: (*a*) $1.327 t_{ff}$; (*b*) $1.364 t_{ff}$; (*c*) $1.379 t_{ff}$; and (*d*) $1.389 t_{ff}$. Each frame shows a region of diameter 6×10^{15} cm spanning 21 radial grid points. Contours correspond to factors of 2 change in density. Maximum densities (log) in g cm^{-3} are noted on each frame. Contours containing density maxima and minima are represented by plus and minus signs, respectively. After forming a weak ring (*a*), the cloud fragments into a binary (*b*), which subsequently subfragments (*c*) into a quadruple system (*d*).

Boss (1993)
Time evolution of disk

- Intermediate angular momentum

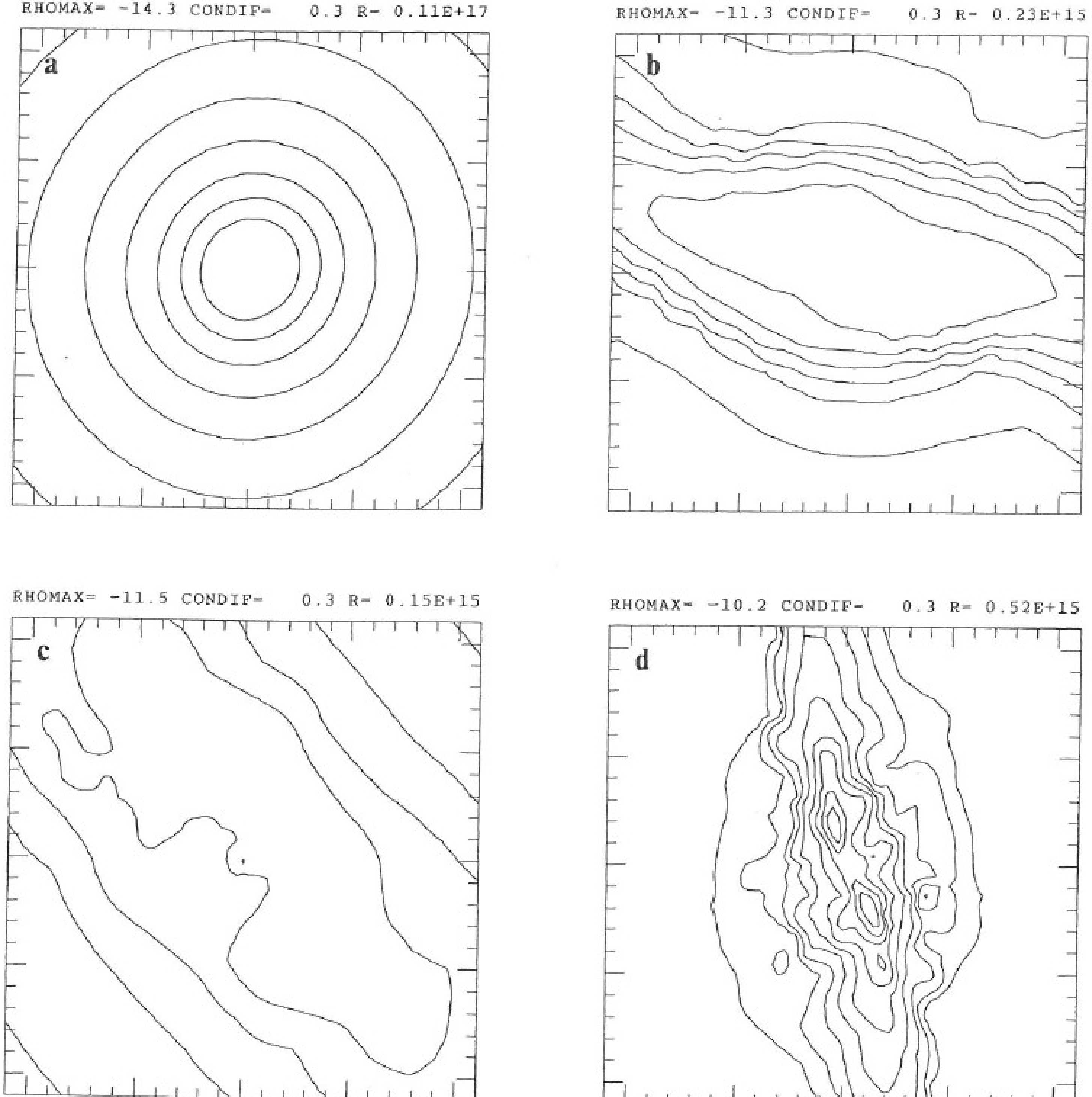

FIG. 5.—Density contours in the equatorial plane for models (*a*) N3 at $1.945t_{ff}$; (*b*) N4 at $1.509t_{ff}$; (*c*) N5 at $1.317t_{ff}$; and (*d*) N7 at $1.211t_{ff}$. Each plot spans 21 adial grid points in diameter, with radii in cm as noted. Model N3 collapsed while remaining single, model N4 formed a single-bar, model N5 formed a binary bar, nd model N7 fragmented into a binary system.

Boss (1993)
Time evolution of disk

- Small angular momentum

Collapse in 3-D

- General results
  - M ↑ → more fragmentation
  - β ↑ → less fragmentation
  - α ↑ → less fragmentation

- Fragmentation always proceeds
  - Never reduced again
- General configuration stable in timescales of 10^7 a
- Inner structure of protostellar cores always dominated by instabilities/fragments

- Isothermal collapse continues to fragment at always smaller scales!

Effects at high densities

- When the dust becomes optically thick, the center warms up
  - T is raised,
  - $M_J \propto \dfrac{T^{3/2}}{\rho^{1/2}}$ increases,
  - fragmentation stops,
  - the core can support itself thermally

$\rightarrow$ Formation of a hydrostatic core

Helmholtz-Kelvin timescale

- Under which conditions does the cloud heat up?
  - Time to radiate gravitational energy away:

$$\tau_{HK} = \frac{GM^2}{R} / L$$

  Helmhotz-Kelvin timescale

  - $\tau_{HK} < \tau_{ff}$ Energy is quickly radiated away $\rightarrow$ isothermal collapse
  - $\tau_{HK} > \tau_{ff}$ Energy is trapped $\rightarrow$ adiabatic collapse

Minimum fragment size

- Fragmentation stops at $\tau_{HK} = \tau_{ff}$
  - Luminosity $L = f \times 4\pi R^2 \sigma T^4$
    - f – grey emission factor ~ 0.1 for dust

$$\frac{GM^2}{4\pi f R^3 \sigma T^4} = \sqrt{\frac{4\pi^2 R^3}{32GM}}$$

$\rightarrow$ critical Jeans mass $M_{J,crit} \approx 0.02 M_\odot \frac{T^{1/4}}{\sqrt{f}}$

- Dust evaporation at T ~ 1000K

$\rightarrow$ $M_{J,crit}$ ~ 0.36 $M_\odot$

Minimum fragment size

- Fragmentation stops at $M_{J,crit} \sim 0.36\ M_\odot$
- Cloud fragment always larger
- Reflected in IMF

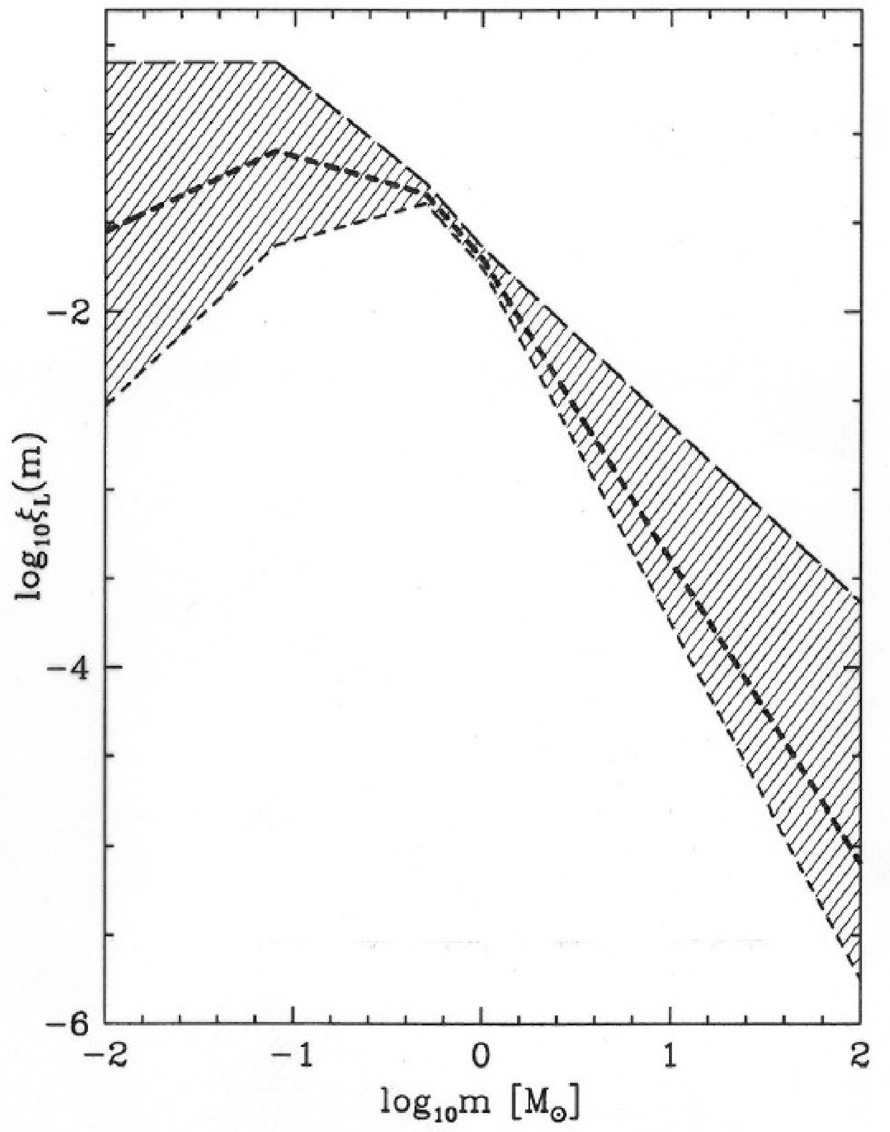

Figure 6.2: The logarithmic IMF. Thick lines show equation 6.1. The shaded region is the range available for the IMF (eqn. 1.12 with $m_2 = m_u$) if it is assumed to be continuous with upper and lower limits on indices given in Fig. 6.1. For $m > 1\,M_\odot$ the range is taken to be the approximate upper and lower bound on the distribution seen in that figure. Specifically: for upper bound on IMF, $\alpha_0 = 1, \alpha_1 = 1.85, \alpha_3 = 2$, while for the lower bound, $\alpha_0 = 0, \alpha_1 = 0.70, \alpha_3 = 3$. In both cases, $\alpha_2 = 2.2$, which is the best-constrained mass-range given the $m(M_v)$ relation (Table 2.6) and the well-determined nearby LF (Table 2.1). The IMF plotted here is scaled to solar-neighbourhood number densities (Kroupa, Tout & Gilmore 1993), the vertical axis being in units of stars/(pc$^3\,M_\odot$).

Effects at high densities

- Collapse can proceed isothermally up to densities of about 10^{10} cm^{-3}
- Then the dust becomes optically thick, infrared radiation cannot escape any more
- Center warms up, fragmentation stops
- Radiation with f=0.1, T=100-1000K, R=2000AU

- Formation of the **first hydrostatic core**

- Slow, adiabatic evolution
  - Temperature increases
  - Density increase very slow

The hydrostatic core

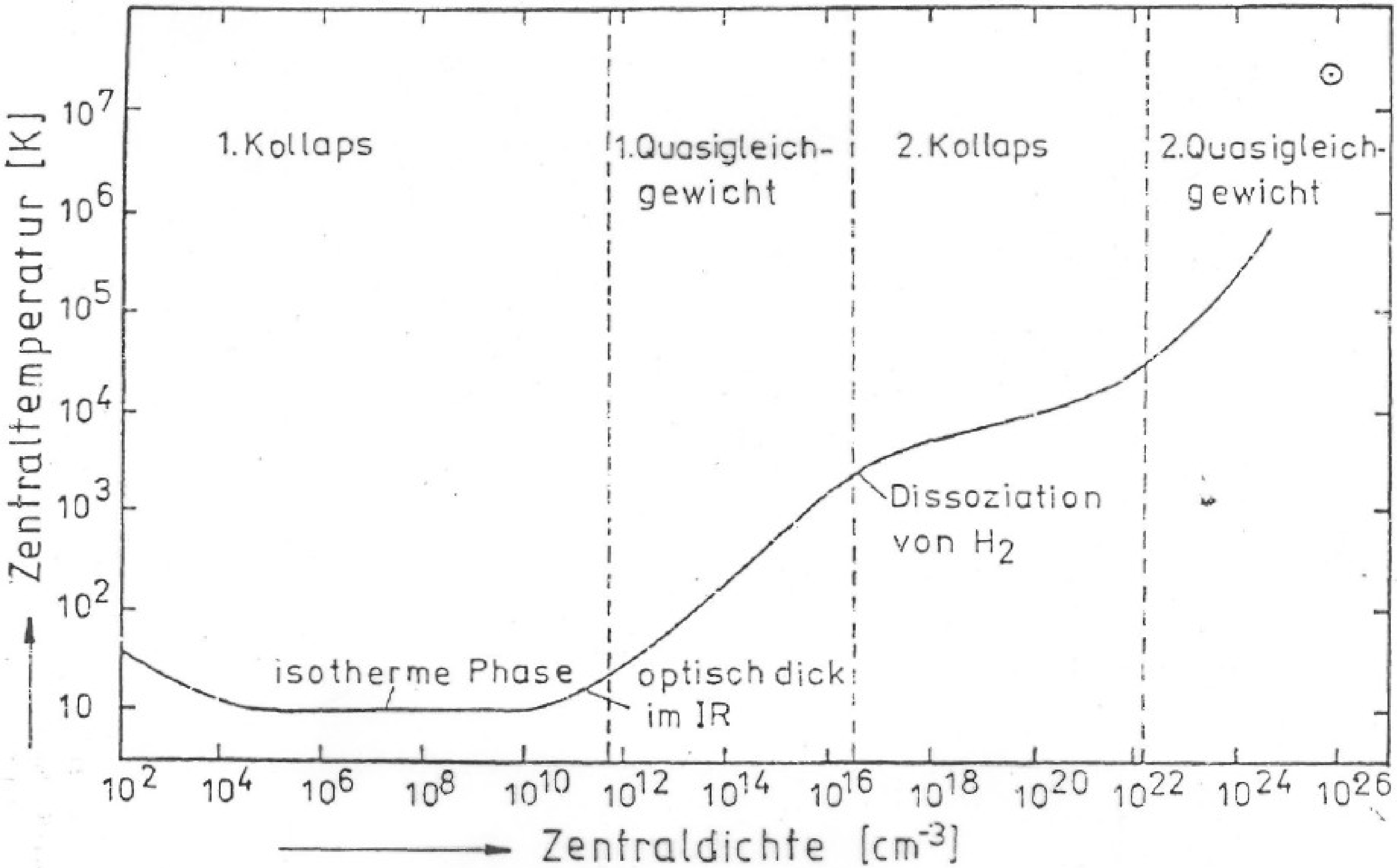

Abbildung 6.3: Zusammenhang zwischen Temperatur und Dichte im Zentrum einer kugelsymmetrischen Wolke während des protostellaren Kollaps'.

Effects at high densities

- The supersonically falling gas falls on the hydrostatic core giving rise to a shock which dominates the protostellar luminosity

$$L_{shock} = \frac{G M_* \dot{M}}{R_*}$$

- When the temperature reaches 1000 K, dust evaporates and cannot contribute to cooling any more
  $\rightarrow$ "opacity gap"

- When the temperature reaches 2000 K, H_2 dissociates

The hydrostatic core

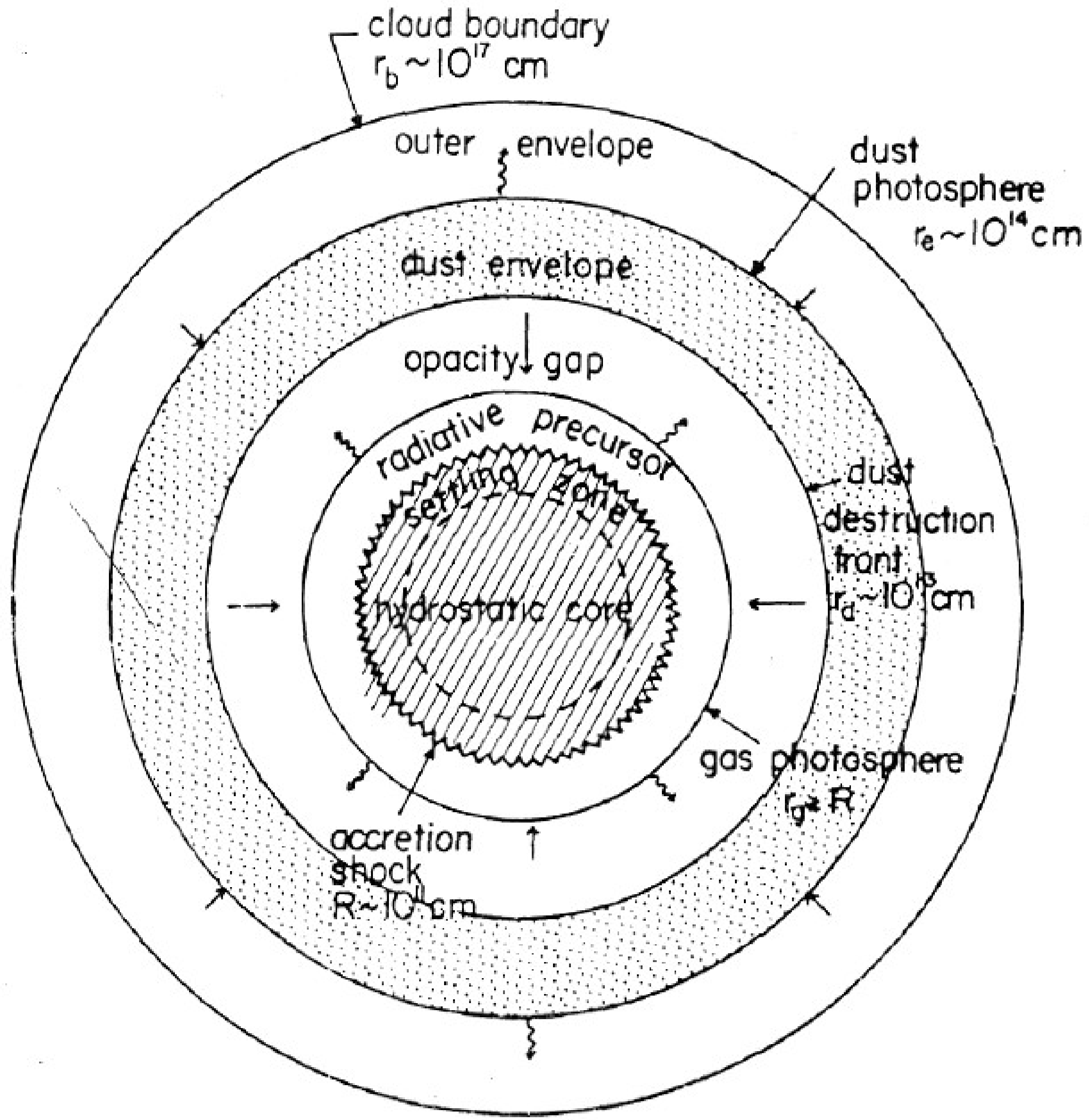

FIG. 1.—The structure of a protostar in the main accretion phase. The dimensions for the various features are given very roughly to aid visualization of the many orders of magnitude of scale involved in this complex problem.

Effects at high densities

- Dissociation of H_2 “consumes” significant amount of energy
  $\rightarrow$ no further heating
  $\rightarrow$ collapse of inner shells can proceed quasi-isothermally

  2nd collapse

- At T>3000K hydrogen is ionized
  - Gas turns optically thick again due to free-free radiation

    $\rightarrow$ **2nd hydrostatic core**

  - Shell structure of evolution combining all effects at different radii

The hydrostatic core

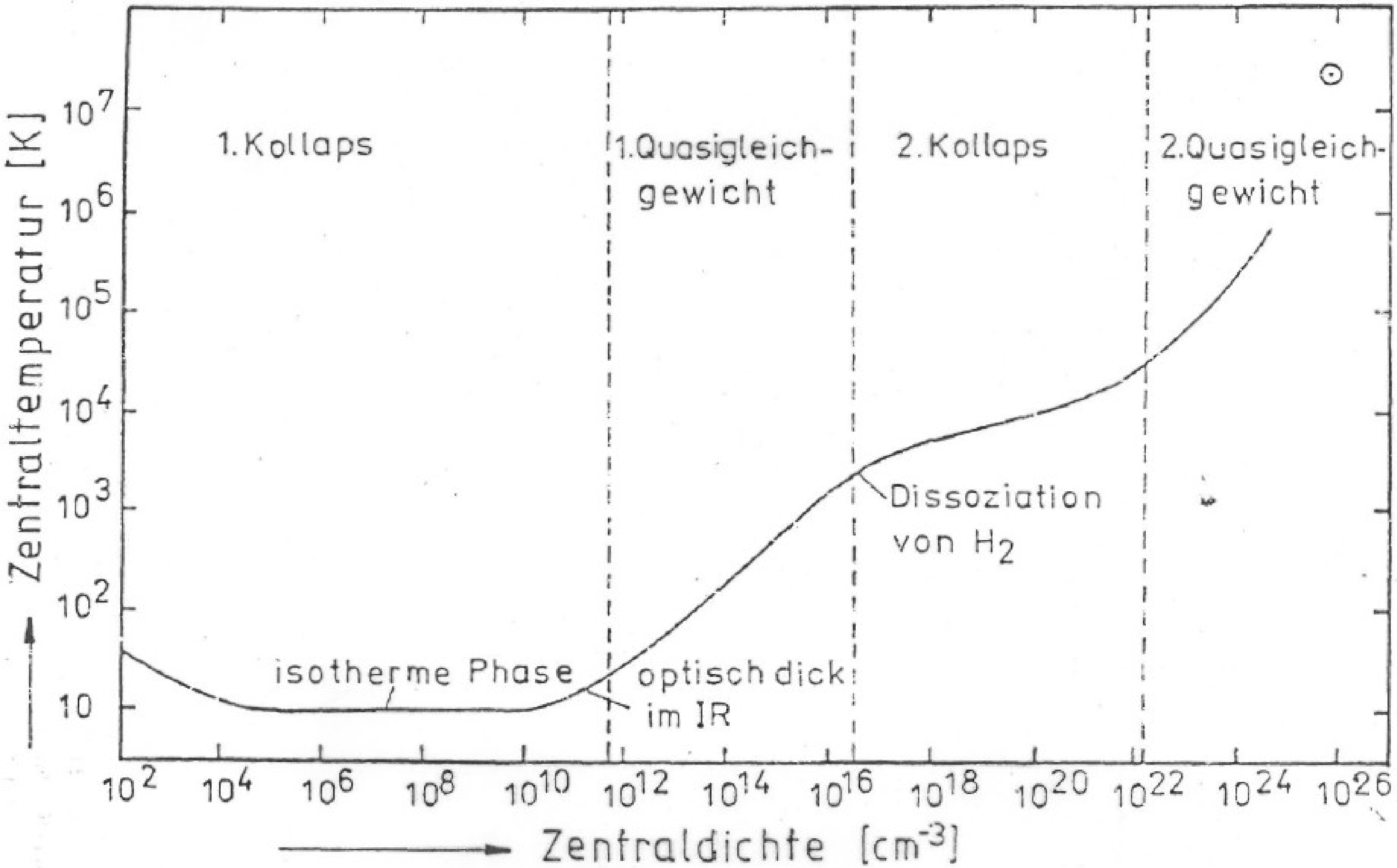

Abbildung 6.3: Zusammenhang zwischen Temperatur und Dichte im Zentrum einer kugelsymmetrischen Wolke während des protostellaren Kollaps'.

The hydrostatic core

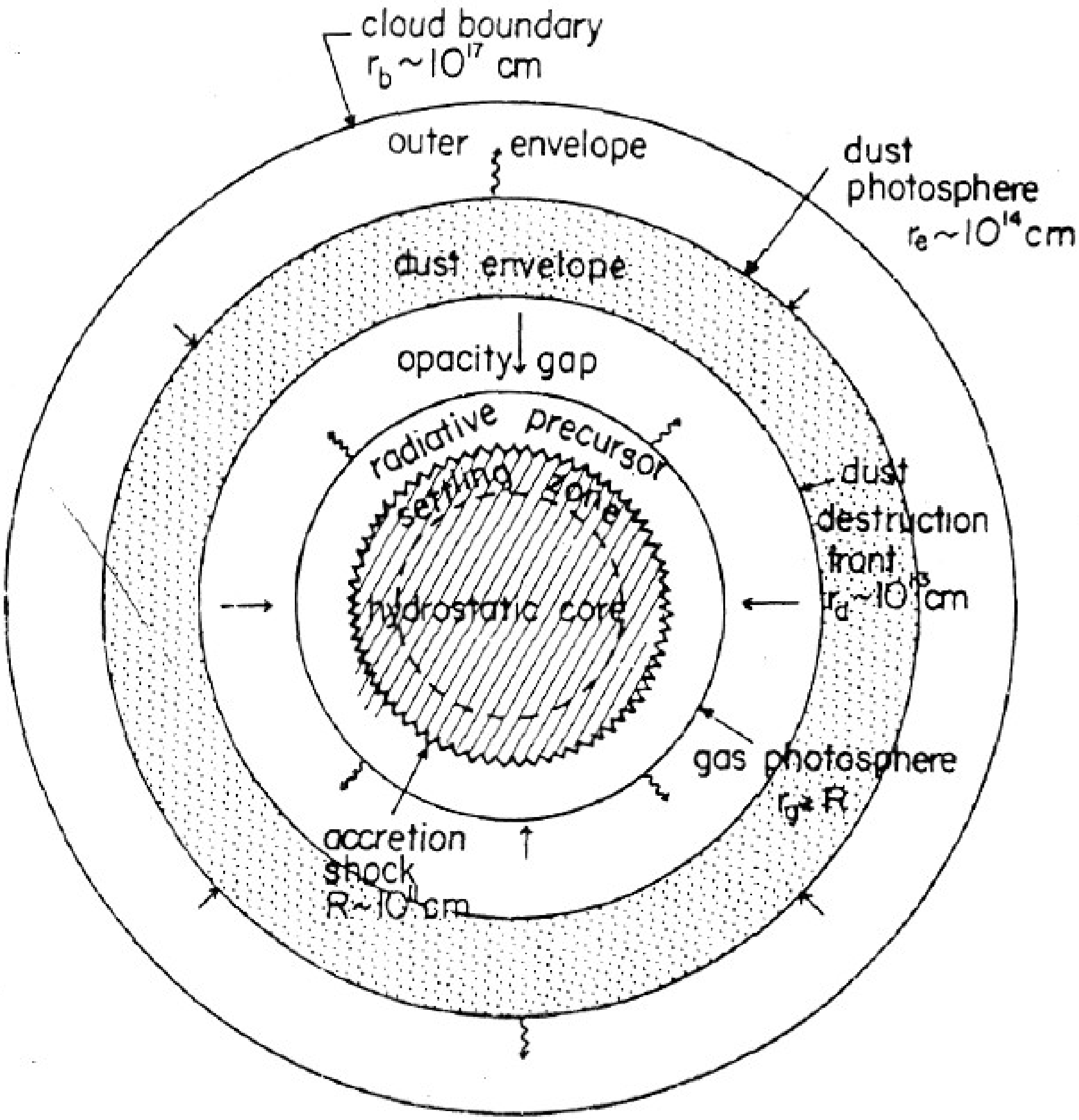

FIG. 1.—The structure of a protostar in the main accretion phase. The dimensions for the various features are given very roughly to aid visualization of the many orders of magnitude of scale involved in this complex problem.